Vegetation History and Archaeobotany (2024) 33:643–655
https://doi.org/10.1007/s00334-024-00988-8

ORIGINAL ARTICLE

Subtropical montane vegetation dynamics in response to Holocene climate change in central Taiwan

Liang-Chi Wang[1,2]

Received: 24 July 2023 / Accepted: 28 October 2023 / Published online: 27 January 2024

Abstract

The East Asian summer monsoon (EASM) is a key component of the global monsoon system, with significant impacts on the climate and ecosystems in Taiwan. However, information about its impact on vegetation diversity during the Holocene in Taiwan and high resolution climate records are unclear and absent. The pollen, charcoal and diatom records from Tien pond are used to provide records with a multidecadal resolution of vegetation changes, fire frequency and hydrological conditions, reflecting the pattern of monsoon intensity and its relationship with subtropical forest ecosystems during the last 8,500 years cal BP. Past temperatures inferred from the percentage of upper montane forest (UMF) taxa and PC2 of principal component analysis (PCA) indicated records of the warm Holocene Thermal Maximum (HTM) during the period 7,000–2,860 cal BP. Past precipitation inferred from diatom concentration and PC1 of PCA showed reduced monsoon precipitation during the thermal maximum. This appears to be the opposite of the pattern in northern China, where the precipitation decreased toward the late Holocene. The positive correlation between the palynological richness index (PRI) and arboreal pollen percentages highlighted the importance of forest canopy cover in driving forest diversity. The high richness in the warm/dry HTM suggests that subtropical montane forests support rich biodiversity and can serve as refugia for taxa during climate fluctuations. These results have implications for conserving and managing subtropical forest ecosystems under future climate change scenarios.

Keywords Pollen · Charcoal · Diatom · Palaeoecology · Conservation · Taiwan

Introduction

The East Asian summer monsoon (EASM) plays a vital role within the global monsoon system, displaying intricate temporal and spatial climate patterns (Zhang et al. 2023). It contributes nearly half of the annual precipitation in East Asia, and any alterations to it can affect the intensity and location of the primary monsoon rain belts and exert significant influences on the ecosystems of Asia. Based on Coupled Modelling Intercomparison Project phase 5/6 models, the monsoon is expected to increase modestly under global warming of 1.5 °C, accompanied by increased water vapour transport. Precipitation in East Asia will increase and there will be significant regional precipitation differences and extreme precipitation events (You et al. 2022). Reconstructing the past development of the EASM is therefore crucial for understanding its response to climate change, assessing its ecological and environmental impacts, and providing empirical evidence and a theoretical foundation for predicting its behaviour in the context of global warming (Zhao et al. 2022, 2023).

Taiwan is situated at the edge of the East Asian continent (Fig. 1A), and the EASM greatly affects its climate. Lake and peat sediments in Taiwan thus provide ideal materials for investigating its past variations. However, conditions of high relief, steep topography, intense rainfall and frequent landslides from typhoons result in high erosion and sedimentation rates. Most sediment records from Taiwan cover only the late Holocene (Wang et al. 2022). Only three sites have sediments that are known to provide coverage for the

Communicated by Y. Zhao.

✉ Liang-Chi Wang
lcwang@ccu.edu.tw

[1] Department of Earth and Environmental Sciences, National Chung Cheng University, Chiayi 62102, Taiwan

[2] Environment and Disaster Monitoring Center, National Chung Cheng University, Chiayi 62102, Taiwan

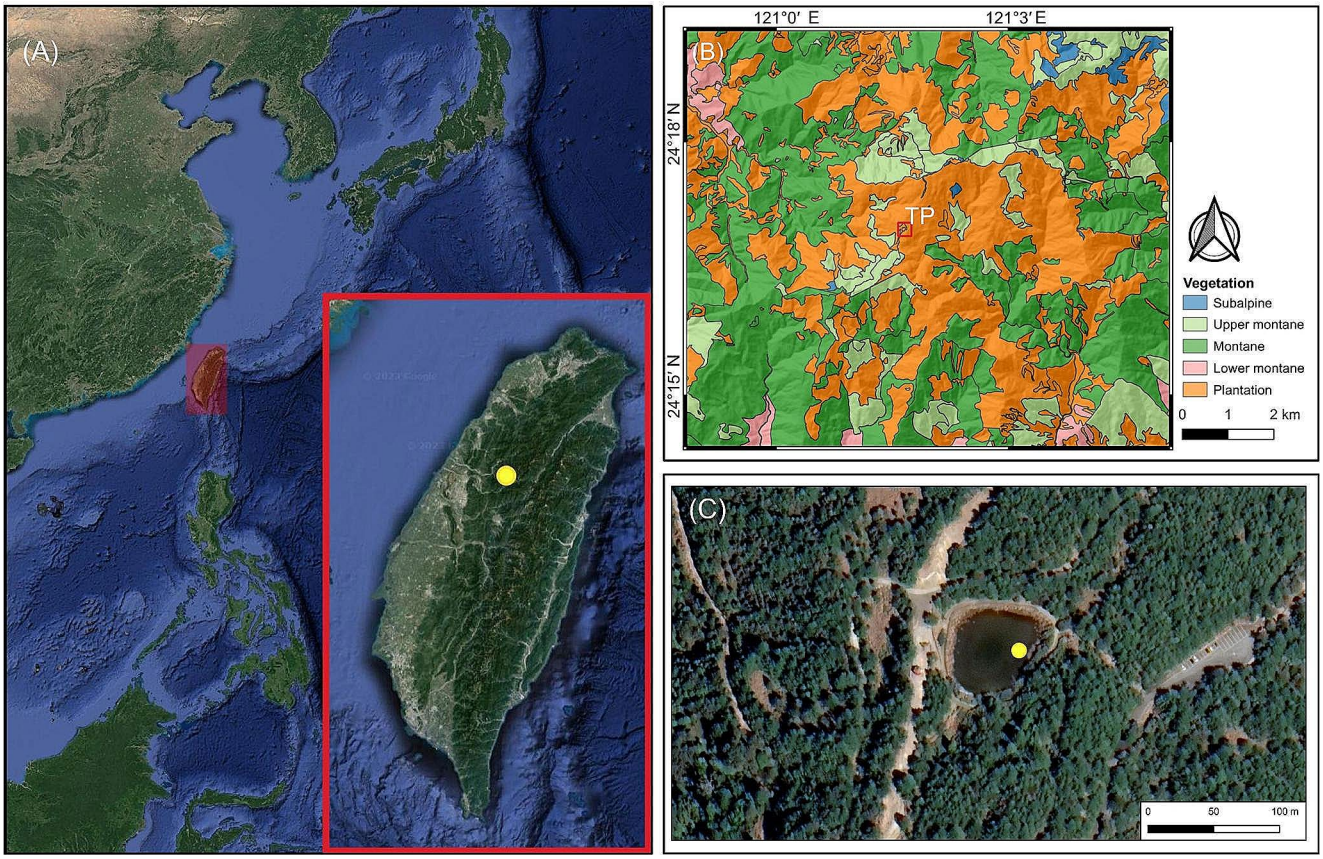

Fig. 1 **A**, location of Tien pond in Taiwan (TP, yellow dot); **B**, local topography and vegetation around TP (red hollow square). Subalpine (blue): cold mountain coniferous forest. Upper montane (pale green): cool-temperate coniferous forest. Montane (dark green): temperate coniferous and broadleaved mixed forest. Lower montane (pink): subtropical broadleaved forest. Plantation (orange): conifer plantations; **C**, satellite photograph of the TP basin and the coring site (yellow dot)

entire Holocene period: Retreat lake (or Chetuei pond) in the montane forest of north-eastern Taiwan (2,230 m a.s.l., the Toushe basin in the lower montane forest of central Taiwan (650 m) and Dongyuan lake in the lowlands of southern Taiwan (360 m). Previous pollen studies at the three sites have provided multi-century records of the variability of the Holocene EASM and its effect on local vegetation (Liew et al. 2006b; Lee et al. 2010; Wang et al. 2014a). However, the scarce and discontinuous temporal record may impede the detection of rapid changes, short-term events, small-scale variations and environmental thresholds (Ding et al. 2020).

This study aims to provide a long-term continuous record of monsoon intensity and its impact on local floristic diversity. To this end, we integrated pollen, charcoal and diatom data from a high altitude site in central Taiwan to reconstruct vegetation history, changes in local plant diversity, wildfire frequency and hydrological conditions (Wang et al. 2020; Wang 2021). Understanding the causes of changes in plant diversity during the Holocene can help to improve the development of nature conservation strategies for subtropical forest ecosystems under climate-warming scenarios.

Materials and methods

Regional setting, coring and subsampling

Tien pond is in mountains at an altitude of 2,600 m in the south-western part of the Xueshan range in central Taiwan (Fig. 1A). It is hydrologically closed, with a surface area of 0.4 ha (Fig. 1C). The bedrock of the TP basin is characterised by Eocene quartz sandstone. The topography is complex, with steep slopes.

According to weather observations from Lishan weather station between 2004 and 2022, the summer monsoon results in a humid subtropical climate in this area (Fig. 2). The local mean annual temperature is 14 °C, ranging from − 1.4 °C in January to 26.9 °C in July. The mean annual rainfall is 2,867 mm, with the most precipitation falling between May and August. The mean annual relative humidity is 83.1%, varying from 78.3 to 88.5%.

Altitude and forest management are the main factors which determine the local vegetation (Li et al. 2013), which can be divided into five communities (Fig. 1B). Above

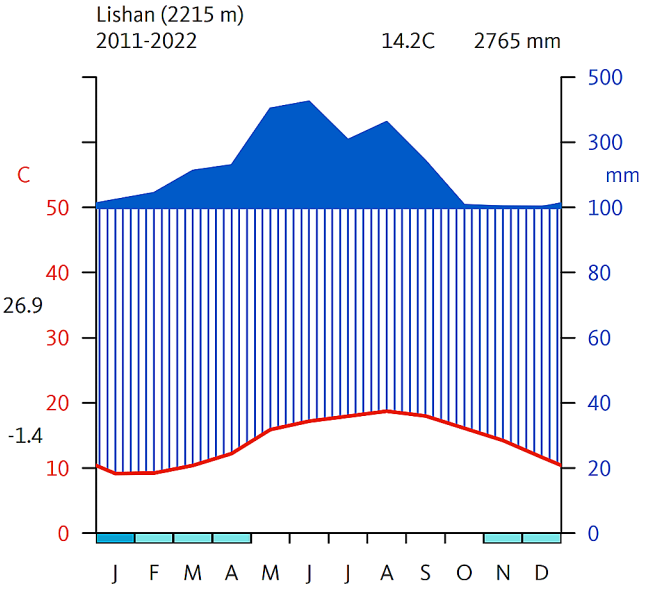

Fig. 2 Walter and Lieth climate diagram of Lishan, the nearest meteorological station to the study site with similar elevation (24°14'51.1"N 121°14'37.2"E, 2,760 m). The diagram shows monthly mean temperature (red line, left y-axis), monthly mean precipitation (blue bars, right y-axis), frost periods (light blue boxes) and probable frost periods (dark blue boxes). The black numbers on the left of the y-axis show the absolute maximum and minimum temperatures. The two black numbers on the right of the top are the annual average temperature and the annual precipitation. The blue filled graph at top indicates wet periods when monthly mean precipitation exceeded 100 mm. The diagram was created by using the climatol package in R (Guijarro 2019)

3,100 m, the vegetation is cold mountain coniferous forest dominated by *Abies kawakamii* (Taiwan fir) and *Yushania niitakayamensis* (niitakayama cane). At 2,500–3,100 m, the vegetation is cool-temperate coniferous forest (upper montane forest, UMF) dominated by *Pinus taiwanensis* (Taiwan red pine) and *Tsuga chinensis* var. *formosana* (Taiwan hemlock). At 1,500–2,500 m, the vegetation is temperate coniferous and broadleaved mixed forest (montane forest, MF). The main tree genera are *Alnus formosana* (Formosan alder), *Chamaecyparis formosensis* (Formosan cypress), *Cyclobalanopsis morii* (oak), *Quercus glauca* (ring-cupped oak) and *Trochodendron aralioides* (wheel tree). Below 1,500 m, the vegetation is subtropical broadleaved forest (lower montane forest, LM) dominated by *Castanopsis cuspidata* var. *carlesii* (long leaf chinquapin). Forestry plantations of *Chamaecyparis formosensis* (Formosan cypress) and *Pinus taiwanensis* (Taiwan red pine) are distributed mainly in the MF. There is no record of human disturbance before the deforestation period between AD 1959 and 1973.

A 250 cm sediment core (DSSTL-2, 24°16'57.9"N, 121°01'39.6"E) was collected in the western part of the pond at a water depth of 30 cm in February 2017, using a Russian-type peat corer. The sediments were subsampled at 2 cm intervals to obtain 125 samples for the analysis of pollen, charcoal and diatoms. The subsamples were kept in a refrigerator 4 °C before chemical treatment.

For radiocarbon dating by the National Taiwan University AMS Laboratory, Taiwan, eight plant remains, two peat and three bulk sediment samples from TP (Table 1) were selected and dried in an oven at 50 °C. The age-depth model of Tien pond was calculated from the AMS radiocarbon dates using the rbacon package in R with the IntCal20 calibration curve (Blaauw and Christen 2011; Reimer et al. 2020).

Pollen, charcoal and diatom analyses

For pollen analysis, a *Lycopodium* spore tablet (batch number 938,934) was added to each 0.5 cm^3 pollen sample to determine the absolute abundance in grains cm^{-3}. The chemical treatment procedure included 10% KOH, 10% HCl, 40% HF and acetolysis. The sample residues were concentrated by sieving on a 5 µm nylon mesh followed by mounting in Kaiser's glycerol gelatin (Riding 2021). The identification and counting of 300 pollen grains per sample were done with a light microscope at 400× magnification, using local pollen and spore floras (Huang 1972, 1981). *Cyclobalanopsis* and *Quercus* were distinguished by their

Table 1 Radiocarbon dates of the samples from the sediment core collected from Tien pond

Laboratory code	Depth (cm)	Type of sample	^{14}C age (cal BP)	Calibrated ^{14}C age (cal BP)
NTUAMS-4104	28–30	Sediment	1,570 ± 19	1,397–1,518
NTUAMS-3747-1	30–34	Plant remains	834 ± 10	716–743
NTUAMS-3748-1	67–68.5	Plant remains	2,230 ± 26	2,151–2,269
NTUAMS-3749-1	87–88	Plant remains	1,965 ± 24	1,828–1,944
NTUAMS-4105	88–90	Sediment	1,724 ± 22	1,544–1,633
NTUAMS-4106	124–126	Peat	2,640 ± 36	2,723–2,789
NTUAMS-4107	141.5–146	Plant remains	3,115 ± 38	3,221–3,401
NTUAMS-3751-1	170–172	Plant remains	3,229 ± 39	3,368–3,494
NTUAMS-4108	174–176	Plant remains	3,022 ± 39	3,138–3,349
NTUAMS-3752-1	178–180	Plant remains	4,603 ± 64	5,208–5,475
NTUAMS-4110	222–224	Peat	7,214 ± 99	7,834–8,208
NTUAMS-4111	240–241	Sediment	7,531 ± 102	8,165–8,544

pollen morphology, which included features like size, polar axis (P)/equatorial diameter (E) ratio and surface ornamentation (Zhang et al. 2018). *Cyclobalanopsis* typically has smaller pollen, measuring < 23 µm, with a P/E ratio of 1.08 and a smooth or finely-grained surface. In contrast, *Quercus* generally has larger pollen exceeding 29 µm, with a P/E ratio of 1.04 and a scabrate pollen surface.

The percentages of pollen and fern spores were calculated from the total pollen sum. Pollen data were subdivided into local pollen assemblage zones using the CONISS cluster analysis program of TiliaGraph (Grimm 1987).

The percentage data of all pollen taxa were used to calculate pollen diversity indices to estimate the changes in vegetation diversity with time and evenness (see below). Studying changes in diversity over time using pollen assemblages is crucial in palaeoecology and ecology. However, conventional diversity indices like Shannon's or Simpson's are unsuitable for analysing pollen percentage data because they both account for the numbers of different taxa and their relative frequencies or representations. Palynological richness can be assessed by simply counting the number of pollen taxa in samples, assuming that sample counts have a standardized number of pollen grains, or through rarefaction analyses (Birks and Line 1992), which was done here to standardize richness estimates across samples of varying sizes by scaling them to a uniform size. The pollen dataset consists of 124 samples with 24 pollen taxa and with sample counts of 330–300 grains. It is important to note that rarefaction serves to interpolate data for sample counts that are smaller than the largest sample in a dataset; it is not capable of extrapolating beyond the highest number of grains found in a sample. Thus, the palynological richness index (PRI) was calculated based on a rarefaction analysis of a pollen count of 300 grains. The probability of interspecific encounter (PIE) is the probability that two individual pollen grains randomly selected from a sample belong to different taxa. It is regarded as an index of palynological evenness (Schwörer et al. 2015).

Only pollen taxa with at least three samples showing > 1% presence were selected for multivariate analysis to reduce the rare taxa effect. Counts of selected pollen taxa were square-root transformed to reduce the impact of dominant taxa and to stabilise the variance (Jantz and Behling 2012). The detrended correspondence analysis (DCA) result showed that the axis length of the first DC axis was 0.75 standard deviations (SD), indicating that linear techniques such as principal component analysis (PCA) were appropriate for analysing the pollen dataset from Tien pond. The diversity estimates and ordination analysis of pollen data were carried out in R using the Vegan and mobr packages (McGlinn et al. 2019).

For the charcoal analysis, samples of 2 cm^3 were treated with 12% NaClO for at least two days to remove the organic materials (Whitlock and Larsen 2001). The samples were then wet-sieved on a 125 µm mesh to separate the charcoal particles. The number of macro-charcoal particles (> 125 µm) was counted under a dissecting microscope to calculate the charcoal concentration (pieces cm^{-3}).

The dynamics of local fires were reconstructed using the CharAnalysis 1.1 code for Matlab (Higuera et al. 2009). The charcoal count data were interpolated to a median time resolution of 50 years, and the interpolated data were log-transformed (log_{10}) to assess the charcoal accumulation rate (CHAR, pieces cm^{-2} yr^{-1}) in constant time steps (C_{inter}). The low frequency variation in CHAR (C_{back}) was used as a locally weighted regression with a 900 year window. The high frequency CHAR (C_{peak}) was calculated as the residual of C_{inter}–C_{back}. C_{peak} consists of C_{noise} (noise from sediment mixing, sampling and analysing) and C_{fire} (actual fire events within 1 km). A Gaussian mixture model was used to identify the C_{noise} distribution, and a 95% threshold was used to separate samples into "fire" and "non-fire" events. The fire frequencies were smoothed using a 900 year window (fires 900 yr^{-1}) to infer the local fire episodes.

For diatom analysis, each sample of 0.5 cm^3 was treated with 10% HCl and 10% H_2O_2 to remove the organic matter and carbonates. The residues were made up to 2 ml with distilled water. Then, a 10 µl subsample of diatom mixture was mounted in Wako Mountmedia to make permanent diatom microscope slides of each sample. The diatom concentration in valves cm^{-3} was calculated by the counts of the diatom valves on one slide with a light microscope at 1,000× magnification.

Results

Lithology and age-depth model

The 250 cm sediment core of TP was divided into six distinct lithological units. The sediment in the upper 25 cm was yellow mud. Below 25 cm, the sediment consisted mainly of two sequential layers of organic-poor white clay and organic-rich dark black peat. A significant transition section between 174 and 182 cm was soil mixed with peat. The 12 radiocarbon dates from the Tien pond deposits spanned the mid to late Holocene, with a bottom sample age of ca. 8,500 cal BP (Table 1; Fig. 3). An age-depth model for the sediment was produced using Bayesian analysis. Three radiocarbon dates were rejected because they did not fit into the age-depth model. On average, the lowest sediment accumulation rate was 280 year cm^{-1} at 174–182 cm. A moderately high accumulation rate of 44 year cm^{-1} was recorded

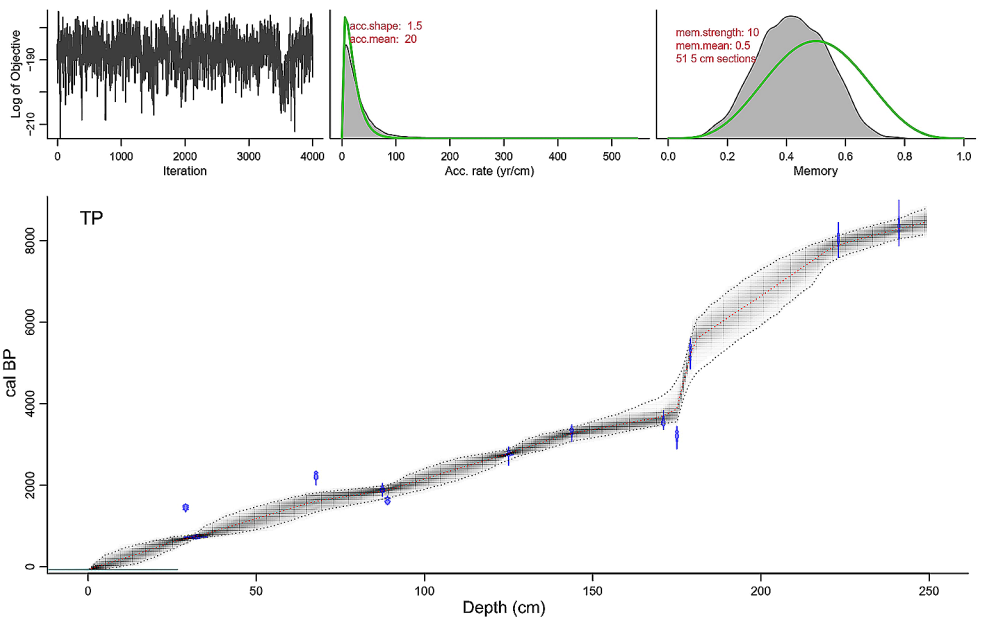

Fig. 3 Age-depth model and lithology for Tien pond created using Bayesian analysis with the rbacon package in R (Blaauw and Christen 2011). The grey shading indicates the 95% probability intervals for the age models. Twelve radiocarbon dates (blue) were used for calibration

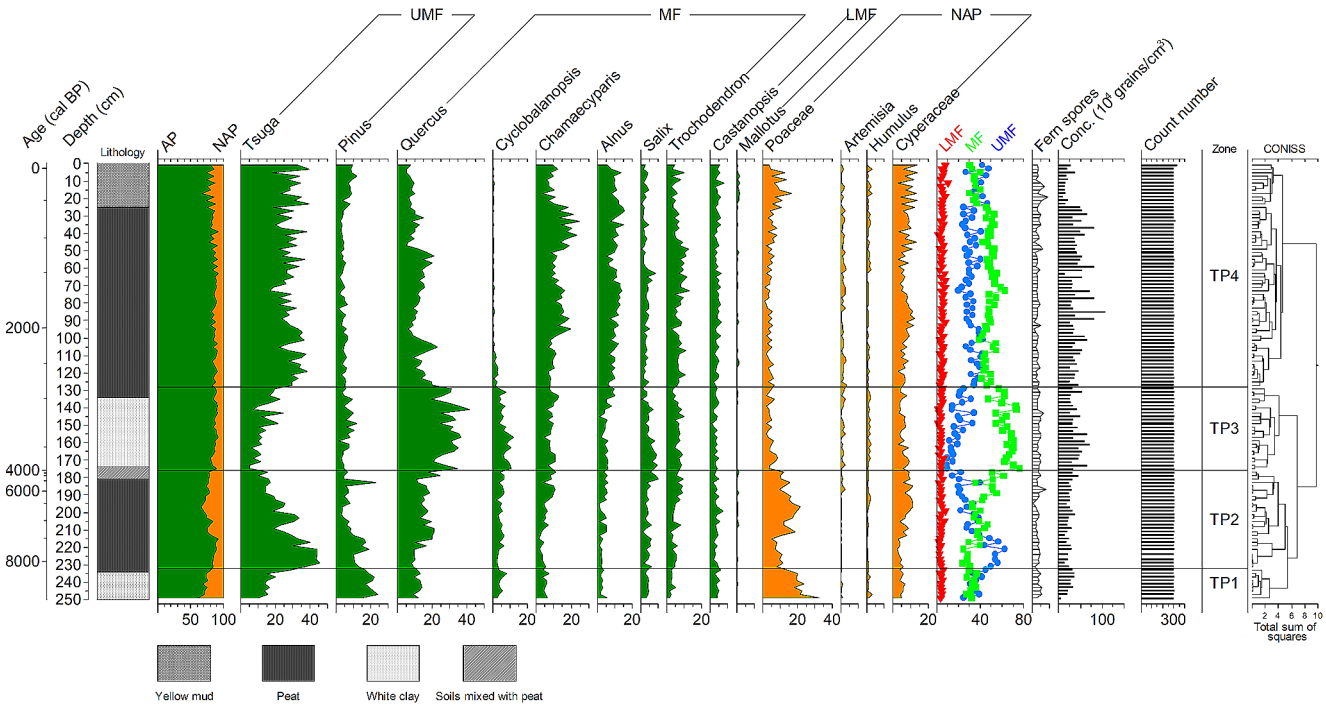

Fig. 4 Lithology and pollen diagram of selected taxa in the sediment cores collected in Tien pond. Percentages are based on the sum of all pollen. UMF = upper montane forest; MF = montane forest; LMF = lower montane forest; Conc. = pollen concentration

between 250 cm and 182 cm and the highest accumulation rate was 23 year cm^{-1} at a depth of 174 cm.

Results

The Tien pond pollen diagram is shown in Fig. 4, with the main pollen taxa in their vegetation types. Four local pollen assemblage zones (TP1–4) were identified based on the CONISS cluster analysis.

TP1 (250–232 cm) was defined by records with a higher percentage of non-arboreal pollen (NAP). Arboreal pollen (AP) dominated with an average of 72%. The upper montane forest (UMF) was the most dominant vegetation type. *Tsuga* (10–28%) and *Pinus* (15–24%) were present at high percentages. Poaceae made up high percentages (14–33%) of NAP, whereas wetland Cyperaceae contributed only 4–7%. The average number of fern spores was 4%. The palynological richness index (PRI) decreased and the probability

of interspecific encounter (PIE) was stable (Fig. 5), and the charcoal accumulation rate (CHAR) was very low. Diatom valves were poorly preserved.

In TP2 (232–176 cm), AP was more abundant than in the previous zone, with an average of 79%. The UMF remained dominant in the lower section but was replaced by montane forest (MF) in the upper section. The UMF taxa *Tsuga* (10–45%) and *Quercus* (8–25%) were dominant. Poaceae (5–21%) increased gradually with a pattern opposite to that of *Tsuga*. Cyperaceae (2–11%) increased slightly. Fern spores remained low, with an average of 3%. PRI and PIE increased gradually. CHAR increased at depths shallower than 200 cm. Diatom valves were still absent.

In TP3 (176–128 cm) MF was the most important vegetation type. *Quercus* (20–41%) and *Cyclobalanopsis* (1–12%) were the dominant tree taxa. NAP was present at a low percentage. Poaceae decreased substantially to an average of 5%. Cyperaceae fluctuated slightly, with an average of 6%. Fern spores increased to 4% on average. The two palynology diversity indices PRI and PIE decreased slightly. CHAR was very high. Diatom valves occurred sporadically at very low concentrations (< 1,000 valves cm^{-3}).

In TP4 (upper 128 cm; 2,860 cal BP to the recent period) AP remained high and the UMF taxon *Tsuga* (17–40%) was relatively important. In the MF, *Chamaecyparis* (7–25%), *Alnus* (5–15%) and *Trochodendron* (3–13%) became more important. Poaceae (1–17%) remained low and showed an increasing trend in the upper 20 cm. Cyperaceae (3–14%) continued to increase. Fern spores increased gradually in the recent period. The palynology diversity indices decreased slightly with relatively strong fluctuations. CHAR was high in the lower section. The diatom concentration was relatively high and showed a pattern opposite to that of the charcoal.

In the principal components analysis, PCA axis 1 (PC1) explained 37.68% of the total variance in the pollen data (Fig. 6) and was related to the local hydrological conditions. The tree taxa *Tsuga*, *Alnus* and *Chamaecyparis* had positive values in PC1, while *Cyclobalanopsis* and *Quercus* had negative values. *Alnus* is a common pioneer element of subtropical mountain forest after landslides (Paolini et al. 2005). In previous pollen studies in Taiwan, the dominance of *Alnus* pollen in sediment records was generally explained by the frequent landslides in mountainous areas resulting from heavy precipitation (Lin et al. 2007; Liew et al. 2014). In addition, wetland Cyperaceae correlated positively with PC1, while correlation with terrestrial herbaceous Poaceae was negative. PC1 may thus be positively associated with the local precipitation in the Tien pond basin. PCA axis 2 (PC2) explained 24.44% of the total variance. The UMF taxa *Tsuga* and *Pinus* had higher positive values, while the MF taxa *Quercus*, *Chamaecyparis*, *Trochodendron* and *Alnus* showed a strong negative correlation. Based on this, the increase in PC2 may imply expansion of upper montane forest, reflecting cold temperatures.

Discussion

Vegetation and palaeoclimate reconstruction

The vegetation history and climate changes in the study area during the Holocene were reconstructed from the proxy data derived from the pollen, charcoal and diatom records (Fig. 7). The relevant pollen source area was correlated with basin shape and size. The Tien pond basin is circular with a radius of approximately 50 m, and pollen deposited there is expected to come from a source area within approximately

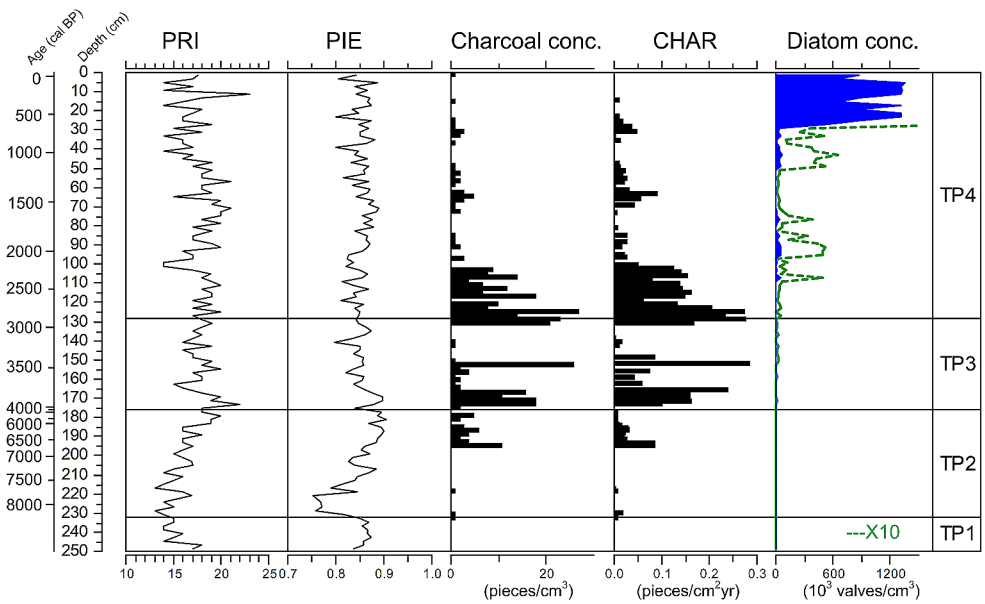

Fig. 5 Profile of the palynological richness index (PRI), probability of interspecific encounter (PIE), charcoal concentration, charcoal accumulation rate (CHAR) and diatom concentration. The green dashed line is a 10x exaggeration of the original values

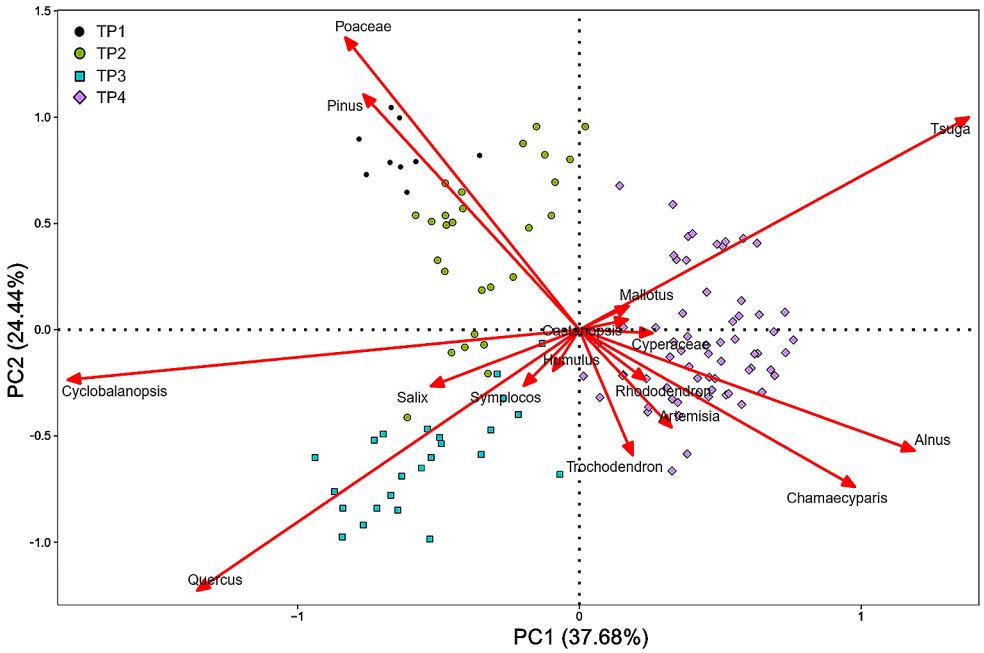

Fig. 6 Principal component analysis (PCA) plot of the two principal axes (PC1 and PC2), including selected pollen taxa and sample scores from Tien pond. Samples are indicated by symbols corresponding to the different pollen zones

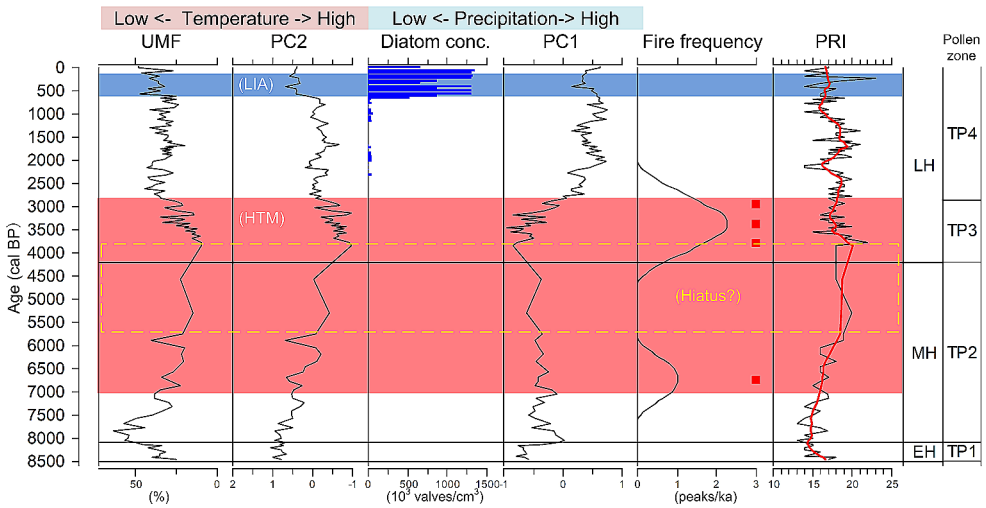

Fig. 7 Summary of the temperature (UMF, PC2), precipitation (diatom conc., PC1), fire frequency and floristic diversity (PRI) of Tien pond during the early Holocene (EH), mid Holocene (MH), and late Holocene (LH). Fire peaks that passed Poisson minimum count screening are indicated with red squares. The red lines of the PRI are smoothed curves generated using the locally weighted scatterplot smoothing method in C2 v. 1.5 for Windows (Juggins 2005). The yellow dashed box indicates a possible hiatus in sediment records. Red bands on the palaeotemperature proxies indicate the warm Holocene Thermal Maximum (HTM) and the blue band indicates the cold Little Ice Age (LIA). UMF = upper montane forest. Diatom conc. = diatom concentration

1,000 m of the basin centre (Sugita 1993; Hjelle and Sugita 2012). Today, Tien pond is located in the upper montane forest zone and is surrounded by dense coniferous forests (Fig. 1B). The increase in UMF correlates with the expansion of the local UMF zone, reflecting a cold climate (Wang et al. 2019; Zhu et al. 2019). Therefore, the UMF percentages and PC2 were used to infer the past temperature. The diatom concentration was used as an index of the change in the water area in Tien pond, and used together with PC1 to show the changes in precipitation there.

Early to mid Holocene

The early Holocene interval (corresponding to TP1, 8,500–8,100 cal BP) was characterised by inorganic white clay sediment. *Pinus taiwanensis* (Taiwan red pine) is the main pine species in subtropical Taiwan. It is a pioneer in forest succession and can grow under poor soil conditions (Zhang 1990; Chen et al. 2016). The high *Pinus* and NAP values suggest an early stage of forest succession and indicate the presence of sparse woods in the Tien pond catchment. The

thin woodland cover may have resulted in intense erosion and increased inputs of inorganic materials into the sediment of the pond.

The high values of UMF and PC2 indicate a cold climate in the early Holocene. The low values of Cyperaceae and PC1 associated with the absence of diatom valves indicate a smaller wetland area and can be attributed to dry conditions. A cold and dry early Holocene is generally consistent with pollen records from Taiwan and is correlated with a weaker East Asian summer monsoon (EASM) (Liew et al. 2006a; Lee and Liew 2010; Wang et al. 2014a).

The lithology change to peat at 8,100 cal BP coincided with a rapid increase in AP, indicating rapid forest expansion during the mid Holocene (corresponding to TP2, 8,100–4,200 cal BP). With the beginning of the mid Holocene, a rapid increase in *Tsuga* pollen indicated the expansion of dense UMF. This was followed by a gradual decrease in UMF, and PC2 suggests an increasing temperature. Wan et al. (2021) recognized major forest expansion in subtropical China since the beginning of the Last Glacial Maximum until the mid Holocene at about 8,100 cal BP, based on high resolution pollen records and model simulations. These authors suggested that the primary expansion of subtropical forest ecosystems was caused by temperature increases when the winter and seasonal temperature contrast crossed a threshold value.

Holocene thermal maximum

From 7,000 to 2,860 cal BP, the composition of AP taxa changed rapidly to MF and was dominated by *Quercus*, *Cyclobalanopsis*, *Chamaecyparis* and *Trochodendron*, reflecting a warm period (Fig. 4). This change in vegetation structure and climate can be correlated with the Holocene thermal maximum (HTM). This was a relatively warm climate phase during the mid to late Holocene, although its timing and spatial pattern varied substantially between different regions, suggesting a varied response to climate and feedback (Renssen et al. 2012). Proxy records from mid and high latitudes of the northern Hemisphere provide evidence of an HTM occurring between 8,000 and 4,000 years ago (Cartapanis et al. 2022). Based on the change in biomes shown by the pollen records, the HTM occurred in central and southern Taiwan from 6,100 to 5,900 cal BP (Liew et al. 2006a; Lee and Liew 2010) and in north-eastern Taiwan from 6,900 to 6,700 cal BP (Wang et al. 2014a), suggesting an intense monsoon in the mid Holocene that reached a maximum in the HTM.

The influence of the HTM is also apparent in several records from the eastern coast of the Asian continent. Adhikari et al. (2002) studied two lake sediment cores collected from Aoki in Japan. Their findings revealed organic contents and diatom abundance that strongly indicated warm conditions there between 7,250 and 6,150 cal BP. Nahm and Hong (2014) analysed palaeoproxy data from three sedimentary cores collected in the Yeongsan river estuary in Korea. Sedimentary features indicated the strong impact of river activity on the sedimentation patterns which suggested relatively wet conditions during the HTM in Korea, specifically from 6,300 to 5,000 cal BP. Overall, these records collectively point to a strong East Asian summer monsoon during the mid Holocene, potentially reaching its peak around 6,100 cal BP, as in the findings of our study.

The low PC1 and the poor preservation of diatom valves suggest dry conditions during this mid to late Holocene period. High NAP values and fire frequency in the thermal maximum suggest the expansion of grassland and an increase in fires, reflecting a dry climate. The significant peak (23%) in *Pinus* at 5,900 cal BP may indicate the start of secondary woodland succession after frequent fire disturbance. Subsequently, the lithology changed to soil for 5,700–3,800 cal BP with an extremely low sedimentation rate (Fig. 3). Warm and dry climate conditions may have increase evaporation and caused the complete drying out of the coring site, resulting in the loss of sediments (Chen et al. 2003). The peak charcoal concentrations in the Toushe basin sediment profile from 5,300 to 4,800 cal BP also indicate this dry phase in central Taiwan (Huang et al. 2020). Thus, this interval was identified as a sedimentary hiatus (Fig. 7).

Poor preservation of diatom valves, a low PC1 value and high fire frequency associated with sediment with little organic content indicate a continuous dry phase from 4,200 to 2,860 cal BP, corresponding to TP3. The differences in the climate reconstruction are from the increased fire frequency in the upper montane forest near the Tien pond basin during this period, resulting in the increased long-distance transport of pollen from montane forest taxa growing at lower altitudes.

Multi proxy data suggest a dry climate at Tien pond during the 4,200–2,860 cal BP period. This result agrees with the decrease in monsoon precipitation, as supported by various long-term climate records in Taiwan (Liew and Hsieh 2000). Evidence includes the rapid reduction in AP pollen in Toushe basin from 4,600 to 3,000 cal BP (Huang et al. 2020), higher percentages of Poaceae pollen in Yuanyang lake from 3,800 to 2,300 cal BP (Chen and Wu 1999), the dominance of *Tsuga* and *Pinus* pollen in Chitsai lake from 3,730 to 2,030 cal BP (Liew and Huang 1994) and charcoal deposits in Hohuanshan mountain with radiocarbon ages of 3,770 and 2,400 cal BP (Wenske et al. 2011). In the marine records, the decreased sediment discharges from Changjiang and Taiwan also indicate a weakening of the monsoon over 5.4–3.0 ka (Zhang et al. 2022).

The charcoal records suggest that fire frequency was low during the hiatus period, but high frequency fire data may have been lost due to the sedimentary gap (Fig. 7). If the charcoal records were continuous across the hiatus, all proxy data would indicate that the temperature and precipitation from 7,000 to 2,860 cal BP were decoupled, reflecting a warm and dry climate. Herzschuh et al. (2019) provide quantitative Holocene precipitation reconstructions based on 101 fossil pollen records from China. The areas of the precipitation patterns and their dates indicate a gradual southward movement and reduced tilt of the westerly jet stream axis since the mid Holocene. This change influenced the summer monsoon rain band, resulting in a precipitation maximum during the early Holocene in most of western China, a mid Holocene maximum in north-central and north-eastern China, and a late Holocene maximum in south-eastern China. The low monsoon precipitation in Taiwan in the Holocene thermal maximum could be the opposite of the trend observed in northern China, where precipitation decreased towards the late Holocene (Kong et al. 2017; Wu et al. 2018).

Climatic oscillations during the last three millennia

The peat layer began to accumulate again between 2,860 and 620 cal BP. The vegetation was characterised by *Tsuga*, *Chamaecyparis* and *Alnus*, indicating the recovery of the local upper montane forest and the expansion of the montane forest. The sedimentation rate increase since 2,860 cal BP indicates that the Tien pond catchment started to receive large amounts of sediment due to rainfall increases (Chen et al. 2018). Diatom valves occurred and PC1 (precipitation) reached a high value at 2,000 cal BP, indicating the expansion of the water area and reflecting stable and high monsoon precipitation. The increased monsoon rainfall during the last two thousand years, although with a reduction of summer sunshine (Lei et al. 2017; Ke et al. 2023), was supported by monsoon proxies in Taiwan (Wang et al. 2015; Wang 2021) and East Asia (Chen et al. 2015). The reversal of the EASM trend over the past 2,000 years could be attributed to the shifting position of the Intertropical Convergence Zone (ITCZ) and the variability of El Niño-Southern Oscillation (ENSO), both of which have been reported to be influenced by changes in summer sunshine in the southern hemisphere and the rise in greenhouse gas concentrations (Zhao et al. 2013; Ding et al. 2020).

The lithology changed to yellow mud at 620 cal BP. The sharp increase in the UMF and PC2 (temperature) indicated a cool phase, corresponding to the Little Ice Age (LIA). The continuously high diatom concentration reveals stable lake conditions, similar to today. The high lake level may relate to high precipitation and low evaporation because of the low temperature. In central mountainous Taiwan, diatom valves in the pond sediment of Tunlumei indicate that the pond area has been stable since 760 cal BP, which also indicates increased precipitation (Wang et al. 2022).

Pinus, *Alnus* and Poaceae have relatively high values during the LIA. *Alnus* is a pioneer taxon on steep landslide slopes and is considered an indicator of typhoon events (Lin et al. 2007; Lee and Tsai 2018). *Pinus* and Poaceae are pioneer secondary plants after disturbances (Chen et al. 2022). Low charcoal values for this period indicated a small number of fire disturbances. In contrast, Cyperaceae values fluctuate strongly, suggesting frequent hydrological variations, such as those caused by typhoons. Frequent typhoons during the LIA have been reported in many palaeolimnological studies in Taiwan and derived from the historical literature of southern China (Chen et al. 2012, 2019; Wang et al. 2013, 2015, 2019, 2022). These authors stated that typhoons hit Japan more often during El Niño-like conditions, while Taiwan is more susceptible to typhoon strikes during La Niña-like phases. The path of typhoons in the north-western Pacific Ocean is influenced by the North Atlantic Oscillation and the Pacific Decadal Oscillation, which had cycles of approximately 30 and 60 years, respectively, during the LIA (Wang et al. 2014b; Chen et al. 2019).

Local floristic diversity and implications for subtropical forest conservation

Climate plays a dominant role in the distribution of plants, influencing their dispersal, migration, evolution, adaptation and even extinction (Pearson and Dawson 2003). At a regional level, mountainous islands like Taiwan have the potential to serve as refuges for taxa during times of climate change. The ample space offered by high mountains facilitates migration of taxa, as probably occurred following the Quaternary glaciations (Hsu and Wolf 2013). However, the potentially suitable areas with high and stable plant species richness will decrease in East Asia under future global warming scenarios (Tang et al. 2018). Thus, the long-term records of local floristic diversity can improve the understanding of the resilience of subtropical forests under different ecological disturbances and inform future conservation practices.

The disturbances from typhoons, human activity and natural fires are potential factors that can impact floristic diversity in Taiwan (He et al. 2019; Wang et al. 2019, 2020). Typhoons significantly impact forest ecosystems, affecting the resilience and diversity of subtropical forests (Lin et al. 2011). However, the palynological richness index (PRI) at Tien pond remained high during the Little Ice Age, a period with frequent typhoons passing through central Taiwan (Chen et al. 2019; Wang et al. 2022), suggesting the

relatively low impact of typhoon disturbances in the Tien pond area.

Evidence of intense human activity is provided by the presence of pollen of cultivated plants and charcoal in the sediments (Lee et al. 2014; Wang et al. 2020). The absence these in the Tien pond sediments indicates a low level of human activity there, and what charcoal is present probably reflects natural wildfires. The idea of minimal human influence near the study site gained support from the observed distribution of archaeological sites in Taiwan and their dates (Leipe et al. 2023). Site numbers in northern, north-eastern and eastern coastal areas of Taiwan increased until approximately 5,000 cal BP. Starting around 3,500 cal BP, there was a significant peak in site numbers in central Taiwan, primarily concentrated in low altitude areas like the Toushe basin, but no prehistoric remains have been found near the Tien pond site.

The significantly opposite pattern of fire frequency and palynological richness indicates that wildfires play a primary role in the variation in forest diversity at Tien pond (Fig. 7). Since there is little sign of any human impact in our record, climate conditions would be expected to be the main factor driving fire frequency. Changes in rainfall patterns, particularly in rainfall levels, tend to coincide with significant fluctuations in the occurrence of fires, because precipitation levels control moisture and thus fire risk (Wenske et al. 2011).

The AP correlated positively with the richness values during the early and mid Holocene. This suggests that forest canopy conditions and precipitation both have a strong influence on forest diversity. Recent studies have demonstrated the crucial role of forest canopy cover in responding to climate change. Closed canopies provide a cooling effect, which slows down changes in the community composition brought about by large climatic changes. In contrast, open canopies accelerate community change through local heating effects (Zellweger et al. 2020).

In addition, the PRI remains high from 7,000 to 4,200 cal BP, which suggests that warming conditions with moderate fire frequency may improve mountain forest diversity (Fig. 7). This indicates that an increase in secondary woods, resulting from wildfires, could enhance plant diversity in subtropical forests in the Holocene Thermal Maximum. In contrast to primary forests, secondary woods tend to have a greater variety of woody plants, higher tree richness, smaller tree sizes, reduced regeneration sizes and a higher proportion of young plants (Chen et al. 2020). Mountainous regions are known for their spatially diverse habitats, which can harbour a rich biodiversity that is especially important during times of climate fluctuations (Meng et al. 2019). Our results indicate that the subtropical montane forest, such as that in the Tien pond area, could provide climate refugia as global warming continues.

Conclusions

The multidecadal pollen, charcoal and diatom records from Tien pond suggest that changes in local vegetation and climate patterns in central mountainous Taiwan during the Holocene were caused mainly by the intensity of the EASM. These climate proxies revealed a gradual increase in EASM intensity from 8,100 to 4,200 cal BP, a decrease from 4,200 to 2,000 cal BP, and another increase during the last 2,000 years. The Holocene Thermal Maximum (HTM) occurred about 7,000–2,860 cal BP with a warm and dry climate. The temperature and monsoonal precipitation are decoupled in the HTM, due to the shift of the westerly jet stream axis, which may influence the summer monsoon rain band. The disturbances caused by typhoons and human activity were insignificant in the TP area. The pollen richness (PRI) correlated negatively with fire frequency and the AP percentages and increased in the HTM. The results indicate that forest canopy cover and fire frequency strongly influence forest diversity, with subtropical montane forests offering spatially diverse habitats that can support rich biodiversity during climate fluctuations, such as global warming.

Acknowledgements I thank Cheng-Jia Jhuang, and Yi-Lin Li for their help in pollen, charcoal, and diatom analysis, Yuan-Pin Chang, Huei-Fen Chen, and Tsai-Wen Lin for their help in core drilling and field excursion. The Dongshih Forest District Office of Taiwan Forestry Bureau is thanked for its permission to sample Tien pond and the National Taiwan University AMS ^{14}C dating laboratory for the radiocarbon measurements. The editor and two anonymous reviewers provided detailed and constructive suggestions which are gratefully acknowledged.

Funding This research was funded by the National Science and Technology Council, Taiwan, grant number 112-2116-M-194 -018-, 111-2116-M-194 -024- and 110-2116-M-194-008-.

Data availability Data will be made available on request.

Declarations

Competing interests The author has no competing interests to declare that are relevant to the content of this article.

References

Adhikari DP, Kumon F, Kawajiri K (2002) Holocene climate variability as deduced from the organic carbon and diatom records in the sediments of Lake Aoki, central Japan. J Geol Soc Jpn 108:249–265. https://doi.org/10.5575/geosoc.108.249

Birks HJB, Line JM (1992) The use of Rarefaction Analysis for estimating Palynological Richness from Quaternary Pollen-Analytical Data. Holocene 2:1–10. https://doi.org/10.1177/095968369200200101

Blaauw M, Christen JA (2011) Flexible paleoclimate age-depth models using an autoregressive gamma process. Bayesian Anal 6:457–474. https://doi.org/10.1214/ba/1339616472

Cartapanis O, Jonkers L, Moffa-Sanchez P et al (2022) Complex spatio-temporal structure of the Holocene Thermal Maximum. Nat Commun 13:5662. https://doi.org/10.1038/s41467-022-33362-1

Chen S-H, Wu J-T (1999) Paleolimnological environment indicated by the diatom and pollen assemblages in an alpine lake in Taiwan. J Paleolimnol 22:149–158

Chen C-TA, Lan H-C, Lou J-Y, Chen Y-C (2003) The Dry Holocene Megathermal in Inner Mongolia. Palaeogeogr Palaeoclimatol Palaeoecol 193:181–200. https://doi.org/10.1016/S0031-0182(03)00225-6

Chen H-F, Wen S-Y, Song S-R et al (2012) Strengthening of paleotyphoon and autumn rainfall in Taiwan corresponding to the Southern Oscillation at late Holocene. J Quat Sci 27:964–972. https://doi.org/10.1002/jqs.2590

Chen R, Shen J, Li C et al (2015) Mid- to late-Holocene East Asian summer monsoon variability recorded in lacustrine sediments from Jingpo Lake, Northeastern China. Holocene 25:454–468. https://doi.org/10.1177/0959683614561888

Chen D, Fang K, Li Y et al (2016) Response of *Pinus taiwanensis* growth to climate changes at its southern limit of Daiyun Mountain, mainland China Fujian Province. Sci China Earth Sci 59:328–336. https://doi.org/10.1007/s11430-015-5188-1

Chen C-W, Oguchi T, Hayakawa YS et al (2018) Sediment yield during typhoon events in relation to landslides, rainfall, and catchment areas in Taiwan. Geomorphology 303:540–548. https://doi.org/10.1016/j.geomorph.2017.11.007

Chen H-F, Liu Y-C, Chiang C-W et al (2019) China's historical record when searching for tropical cyclones corresponding to Intertropical Convergence Zone (ITCZ) shifts over the past 2kyr. Clim Past 15:279–289. https://doi.org/10.5194/cp-15-279-2019

Chen X, Wang X, Li J, Kang D (2020) Species diversity of primary and secondary forests in Wanglang Nature Reserve. Glob Ecol Conserv 22:e01022. https://doi.org/10.1016/j.gecco.2020.e01022

Chen C, Zhao W, Xia Y et al (2022) History of human disturbance to vegetation in the Southeast Hills of China over the last 2900 years: evidence from a high resolution pollen record. Palaeogeogr Palaeoclimatol Palaeoecol 598:111028. https://doi.org/10.1016/j.palaeo.2022.111028

Ding X, Zheng L, Zheng X, Kao S-J (2020) Holocene East Asian Summer Monsoon Rainfall variability in Taiwan. Front Earth Sci 8:234. https://doi.org/10.3389/feart.2020.00234

Grimm EC (1987) CONISS: a FORTRAN 77 program for stratigraphically constrained cluster analysis by the method of incremental sum of squares. Comput Geosci 13:13–35

Guijarro JA (2019) Package 'climatol'. https://CRAN.R-project.org/package=climatol. Retrieved 2004, 2020

He T, Lamont BB, Pausas JG (2019) Fire as a key driver of Earth's biodiversity. Biol Rev 94:1:983–2010. https://doi.org/10.1111/brv.12544

Herzschuh U, Cao X, Laepple T et al (2019) Position and orientation of the westerly jet determined Holocene rainfall patterns in China. Nat Commun 10:2376. https://doi.org/10.1038/s41467-019-09866-8

Higuera PE, Brubaker LB, Anderson PM et al (2009) Vegetation mediated the impacts of postglacial climate change on fire regimes in the south-central Brooks Range, Alaska. Ecol Monogr 79:201–219. https://doi.org/10.1890/07-2019.1

Hjelle KL, Sugita S (2012) Estimating pollen productivity and relevant source area of pollen using lake sediments in Norway: How does lake size variation affect the estimates? Holocene 22:313–324. https://doi.org/10.1177/0959683611423690

Hsu RC-C, Wolf JHD (2013) A Novel Approach to Simulate Climate Change impacts on vascular epiphytes: Case Study in Taiwan. In: Lowman M, Devy S, Ganesh T (eds) Treetops at risk: challenges of Global Canopy Ecology and Conservation. Springer, New York, pp 123–130

Huang T-C (1972) Pollen Flora of Taiwan. National Taiwan University, Botany Department Press, Taipei, p 297

Huang T-C (1981) Spore Flora of Taiwan. National Taiwan University Botany Department Press, Taipei, p 111

Huang Z, Ma C, Chyi S-J et al (2020) Paleofire, vegetation, and climate reconstructions of the Middle to Late Holocene from lacustrine sediments of the Toushe Basin, Taiwan. Geophys Res Lett 47:e2020GL090401. https://doi.org/10.1029/2020GL090401

Jantz N, Behling H (2012) A Holocene environmental record reflecting vegetation, climate, and fire variability at the Páramo of Quimsacocha, southwestern Ecuadorian Andes. Veget Hist Archaeobot 21:169–185. https://doi.org/10.1007/s00334-011-0327-x

Juggins S (2005) C2 Version 1.5: software for ecological and palaeoecological data analysis and visualisation. University of Newcastle, Newcastle

Ke R, Xiao X, Chi C et al (2023) Middle-late Holocene environment change induced by climate and human based on multi-proxy records from the middle and lower reaches of Yangtze River, eastern China. Sci China Earth Sci 66:1,450–1,467. https://doi.org/10.1007/s11430-022-1101-2

Kong W, Swenson LM, Chiang JCH (2017) Seasonal transitions and the westerly jet in the Holocene East Asian summer monsoon. J Clim 30:3,343–3,365

Lee C-Y, Liew P-M (2010) Late quaternary vegetation and climate changes inferred from a pollen record of Dongyuan Lake in southern Taiwan. Palaeogeogr Palaeoclimatol Palaeoecol 287:58–66. https://doi.org/10.1016/j.palaeo.2010.01.015

Lee J-T, Tsai S-M (2018) The nitrogen-fixing Frankia significantly increases growth, uprooting resistance and root tensile strength of *Alnus formosana*. Afr J Biotechnol 17:213–225. https://doi.org/10.5897/AJB2017.16289

Lee C-Y, Liew P-M, Lee T-Q (2010) Pollen records from southern Taiwan: implications for east Asian summer monsoon variation during the Holocene. Holocene 20:81–89. https://doi.org/10.1177/0959683609348859

Lee C-Y, Chang C-L, Liew P-M et al (2014) Climate change, vegetation history, and agricultural activity of Lake Li-yu Tan, central Taiwan, during the last 2.6 ka BP. Quat Int 325:105–110. https://doi.org/10.1016/j.quaint.2013.05.029

Lei G, Zhu Y, Cai B et al (2017) Mid-late Holocene climate variations in southeast China inferred by the intermountain peat records from Fujian, China. Quat Int 447:118–127. https://doi.org/10.1016/j.quaint.2016.09.051

Leipe C, Lu J, Chi K (2023) Population dynamics in Taiwan from the Neolithic to early historic periods (5000–100 cal BP): linking cultural developments and environmental change. Archaeol Res Asia 36:100482. https://doi.org/10.1016/j.ara.2023.100482

Li C-F, Chytrý M, Zelený D et al (2013) Classification of Taiwan forest vegetation. Appl Veg Sci 16:698–719. https://doi.org/10.1111/avsc.12025

Liew P-M, Hsieh M-L (2000) Late Holocene (2 ka) sea level, river discharge and climate interrelationship in the Taiwan region. J Asian Earth Sci 18:499–505. https://doi.org/10.1016/S1367-9120(99)00081-4

Liew P-M, Huang S-Y (1994) A 5000 year pollen record from Chitsai Lake in Central Taiwan. Terr Atmos Ocean Sci 5:411–419

Liew P-M, Huang S-Y, Kuo C-M (2006a) Pollen stratigraphy, vegetation and environment of the last glacial and Holocene – A record from Toushe Basin, central Taiwan. Quat Int 147:16–33

Liew P-M, Lee C-Y, Kuo C-M (2006b) Holocene thermal optimal and climate variability of east Asian monsoon inferred from forest reconstruction of a subalpine pollen sequence, Taiwan. Earth Planet Sci Lett 250:596–605. https://doi.org/10.1016/j.epsl.2006.08.002

Liew P-M, Wu M-H, Lee C-Y et al (2014) Recent 4000 years of climatic trends based on pollen records from lakes and a bog in Taiwan. Quat Int 349:105–112. https://doi.org/10.1016/j.quaint.2014.05.018

Lin S-F, Huang T-C, Liew P-M, Chen S-H (2007) A palynological study of environmental changes and their implication for prehistoric settlement in the Ilan Plain, northeastern Taiwan. Veget Hist Archaeobot 16:127–138

Lin T-C, Hamburg SP, Lin K-C et al (2011) Typhoon disturbance and forest dynamics: lessons from a Northwest Pacific subtropical forest. Ecosystems 14:127–143

McGlinn DJ, Xiao X, May F et al (2019) Measurement of Biodiversity (MoB): a method to separate the scale-dependent effects of species abundance distribution, density, and aggregation on diversity change. Methods Ecol Evol 10:258–269. https://doi.org/10.1111/2041-210X.13102

Meng H-H, Zhou S-S, Jiang X-L et al (2019) Are mountaintops climate refugia for plants under global warming? A lesson from high-mountain oaks in tropical rainforest. Alp Bot 129:175–183. https://doi.org/10.1007/s00035-019-00226-2

Nahm W-H, Hong S-S (2014) Holocene environmental changes inferred from sedimentary records in the lower reach of the Yeongsan River, Korea. Holocene 24:1,798–1,809. https://doi.org/10.1177/0959683614551221

Paolini L, Villalba R, Grau HR (2005) Precipitation variability and landslide occurrence in a subtropical mountain ecosystem of NW Argentina. Dendrochronologia 22:175–180. https://doi.org/10.1016/j.dendro.2005.06.001

Pearson RG, Dawson TP (2003) Predicting the impacts of climate change on the distribution of species: Are bioclimate envelope models useful? Glob Ecol Biogeogr 12:361–371. https://doi.org/10.1046/j.1466-822X.2003.00042.x

Reimer PJ, Austin WEN, Bard E et al (2020) The IntCal20 Northern Hemisphere Radiocarbon Age Calibration curve (0–55 cal kBP). Radiocarbon 62:725–757. https://doi.org/10.1017/RDC.2020.41

Renssen H, Seppä H, Crosta X et al (2012) Global characterization of the Holocene Thermal Maximum. Quat Sci Rev 48:7–19. https://doi.org/10.1016/j.quascirev.2012.05.022

Riding JB (2021) A guide to preparation protocols in palynology. Palynology 45:1–110. https://doi.org/10.1080/01916122.2021.1878305

Schwörer C, Colombaroli D, Kaltenrieder P et al (2015) Early human impact (5000–3000 BC) affects mountain forest dynamics in the Alps. J Ecol 103:281–295. https://doi.org/10.1111/1365-2745.12354

Sugita S (1993) A model of pollen source area for an entire lake surface. Quat Res 39:239–244

Tang CQ, Matsui T, Ohashi H et al (2018) Identifying long-term stable refugia for relict plant species in East Asia. Nat Commun 9:4488. https://doi.org/10.1038/s41467-018-06837-3

Wan Q, Zhang X, Zhang Y et al (2021) Major Forest changes in Subtropical China since the last ice age. Forests 12:1314. https://doi.org/10.3390/f12101314

Wang L-C (2021) Using Paleoecological Data to inform the Conservation Strategy for Floristic Diversity and *Isoetes taiwanensis* in Northern Taiwan. Diversity 13:395. https://doi.org/10.3390/d13080395

Wang L-C, Behling H, Lee T-Q et al (2013) Increased precipitation during the little ice age in northern Taiwan inferred from diatoms and geochemistry in a sediment core from a subalpine lake. J Paleolimnol 49:619–631. https://doi.org/10.1007/s10933-013-9679-9

Wang L-C, Behling H, Chen Y-M et al (2014a) Holocene monsoonal climate changes tracked by multiproxy approach from a lacustrine sediment core of the subalpine Retreat Lake in Taiwan. Quat Int 333:69–76

Wang L-C, Behling H, Lee T-Q et al (2014b) Late Holocene environmental reconstructions and their implications on flood events, typhoon, and agricultural activities in NE Taiwan. Clim Past 10:1857–1869. https://doi.org/10.5194/cp-10-1857-2014

Wang L-C, Behling H, Kao S-J et al (2015) Late Holocene environment of subalpine northeastern Taiwan from pollen and diatom analysis of lake sediments. J Asian Earth Sci 114:447–456. https://doi.org/10.1016/j.jseaes.2015.03.037

Wang L-C, Tang Z-W, Chen H-F et al (2019) Late Holocene vegetation, climate, and natural disturbance records from an alpine pond in central Taiwan. Quat Int 528:63–72. https://doi.org/10.1016/j.quaint.2019.03.005

Wang L-C, Chang Y-P, Li H-C et al (2020) Revealing the vegetation, fire and human activities in the lowland of eastern Taiwan during late Holocene. Quat Int 544:32–40. https://doi.org/10.1016/j.quaint.2018.08.003

Wang L-C, Chou Y-M, Chen H-F et al (2022) Paleolimnological evidence for lacustrine environmental evolution and paleo-typhoon records during the late Holocene in eastern Taiwan. J Paleolimnol 68:7–23. https://doi.org/10.1007/s10933-020-00153-x

Wenske D, Böse M, Frechen M, Lüthgens C (2011) Late Holocene mobilisation of loess-like sediments in Hohuan Shan, high mountains of Taiwan. Quat Int 234:174–181. https://doi.org/10.1016/j.quaint.2009.10.034

Whitlock C, Larsen C (2001) Charcoal as a Fire Proxy. In: Smol JP, Birks HJB, Last WM, Bradley RS, Alverson K (eds) Tracking Environmental Change using Lake sediments, vol 3:Terrestrial, Algal, and Siliceous indicators. Kluwer Academic Publishers, Dordrecht, pp 75–97

Wu D, Chen X, Lv F et al (2018) Decoupled early Holocene summer temperature and monsoon precipitation in southwest China. Quat Sci Rev 193:54–67. https://doi.org/10.1016/j.quascirev.2018.05.038

You Q, Jiang Z, Yue X et al (2022) Recent frontiers of climate changes in East Asia at global warming of 1.5°C and 2°C. Npj Clim Atmos Sci 5:80. https://doi.org/10.1038/s41612-022-00303-0

Zellweger F, De Frenne P, Lenoir J et al (2020) Forest microclimate dynamics drive plant responses to warming. Science 368:772–775. https://doi.org/10.1126/science.aba6880

Zhang L (1990) Population structure and dynamics of *Pinus taiwanensis* Hayata at Songyang County, Zhejiang Province, China. Vegetatio 86:119–129. https://doi.org/10.1007/BF00031728

Zhang X, Huang K-Y, Zheng Z et al (2018) Pollen morphology of *Quercus* sect. *Ilex* and its relevance for fossil pollen identification in southwest China. Grana 57:401–414. https://doi.org/10.1080/00173134.2018.1480653

Zhang S, Liu S, Shu Z et al (2022) Climate-driven provenance variation and sedimentary system evolution at the Changjiang distal mud since the mid-Holocene. Mar Geol 452:106902. https://doi.org/10.1016/j.margeo.2022.106902

Zhang X, Liu J, Rühland KM et al (2023) Concurrent mid-Holocene East Asian temperature and summer monsoon maxima forced by high- and low-latitude interplay. Glob Planet Chang 220:104008. https://doi.org/10.1016/j.gloplacha.2022.104008

Zhao C, Chang Y-P, Chen M-T, Liu Z (2013) Possible reverse trend in Asian summer monsoon strength during the late Holocene. J Asian Earth Sci 69:102–112. https://doi.org/10.1016/j.jseaes.2012.09.028

Zhao L, Ma C, Wen Z et al (2022) Vegetation dynamics and their response to Holocene climate change derived from multi-proxy records from Wangdongyang peat bog in southeast China.

Veget Hist Archaeobot 31:247–260. https://doi.org/10.1007/s00334-021-00852-z

Zhao J, Liu J, Liu J et al (2023) Coupling of the ecosystems in North China with the east Asian summer monsoon rainfall during the Holocene. Quat Sci Rev 300:107885. https://doi.org/10.1016/j.quascirev.2022.107885

Zhu Y, Lei G, Li Z et al (2019) Montane peat bog records of vegetation, climate, and human impacts in Fujian Province, China, over the last 1330 years. Quat Int 528:53–62. https://doi.org/10.1016/j.quaint.2019.04.016